Another Look at Zonal Flows: Resonance, Shearing and Frictionless Saturation

J. C. Li[1] and P. H. Diamond[1]

[1]*CASS, University of California, San Diego, California 92093, USA*

Abstract

We show that shear is not the exclusive parameter that represents all aspects of flow structure effects on turbulence. Rather, wave–flow resonance enters turbulence regulation, both linearly and nonlinearly. Resonance suppresses the linear instability by wave absorption. Flow shear can weaken the resonance, and thus destabilize drift waves, in contrast to the near-universal conventional shear suppression paradigm. Furthermore, consideration of wave–flow resonance resolves the long-standing problem of how zonal flows (ZF) saturate in the limit of weak or zero frictional drag, and also determines the ZF scale. We show that resonant vorticity mixing, which conserves potential enstrophy, enables ZF saturation in the absence of drag, and so is effective at regulating the Dimits up-shift regime. Vorticity mixing is incorporated as a nonlinear, self-regulation effect in an *extended* 0D predator–prey model of drift–ZF turbulence. This analysis determines the saturated ZF shear and shows that the mesoscopic ZF width scales as $L_{ZF} \sim f^{3/16}(1-f)^{1/8}\rho_s^{5/8}l_0^{3/8}$ in the (relevant) adiabatic limit (i.e., $\tau_{ck}k_\parallel^2 D_\parallel \gg 1$). f is the fraction of turbulence energy coupled to ZF and l_0 is the base state mixing length, absent ZF shears. We calculate and compare the stationary flow and turbulence level in frictionless, weakly frictional, and strongly frictional regimes. In the frictionless limit, the results differ significantly from conventionally quoted scalings derived for frictional regimes. To leading order, the flow is independent of turbulence intensity. The turbulence level scales as $E \sim (\gamma_L/\varepsilon_c)^2$, which indicates the extent of the "near-marginal" regime to be $\gamma_L < \varepsilon_c$, for the case of avalanche-induced profile variability. Here, ε_c is the rate of dissipation of potential enstrophy and γ_L is the characteristic linear growth rate of fluctuations. The implications for dynamics near marginality of the strong scaling of saturated E with γ_L are discussed.

I. INTRODUCTION

Zonal flows (ZF) are very effective at regulating drift wave (DW) turbulence, as they are the secondary modes of minimal inertia, transport, and damping[1, 2]. Such a mechanism naturally can be thought of as an element in a 'predator–prey' type ecology[3, 4], in which the secondary 'predator' feeds off (i.e., extracts energy from) of the primary 'prey'. In such a system, the damping of the predator (here, the ZF) ultimately regulates the full system. Frictional drag, due to collisions, is usually invoked to damp ZF. However, this picture is unsatisfactory for present day and future regimes of low collisionality. Thus, it becomes essential to understand *frictionless* ZF saturation and its implications for drift wave turbulence. Of course, ZF saturation significantly impacts transport and turbulence scalings. Note that understanding scalings in the frictionless regime is essential for developing reduced models thereof. As zonal flow shear reduces the turbulent mixing scale, the saturated zonal flow is coupled to the scaling of turbulent diffusivity with $\rho_* \equiv \rho_s/L_n$. This is related to the degree of gyro-Bohm breaking[5], i.e. the exponent α in $D \sim D_B \rho_*^\alpha$, where $D_B \equiv k_B T/16eB$ is Bohm diffusivity and $\alpha < 1$ indicates gyro-Bohm breaking.

Related to zonal flow saturation, we note that strong resonance between drift waves and azimuthal (i.e., zonal) flow is observed in a linear device CSDX (Controlled Shear Decorrelation eXperiment), i.e. $\omega_k - k_\theta \langle v_\theta \rangle \ll \omega_{*e}$, with ω_{*e} being the electron drift frequency. CSDX is a well-diagnosed venue to study the interaction between turbulence and turbulence driven flows in straight magnetic fields[6, 7]. Though resonance is manifested most clearly in the linear device, it has more general implications for confinement devices.

Wave-flow resonance enters turbulence regulation by zonal flows both linearly and nonlinearly. Resonance alters our understanding of the shear suppression mechanisms. To this end, the effects of $E \times B$ shear flows on turbulence have been intensively studied. However, simplified shear suppression models are *not* universally applicable. In some limits, weak flow shear can even destabilize turbulence due to the coupling of radial eigenmodes[8]. Moreover, flow shearing alone is not the only parameter that characterizes all effects of flow structure on turbulence[9]. For example, wave-flow resonance stabilizes turbulence through wave absorption[8, 10]. Yet, resonance is often overlooked by many existing shear suppression models.

Resonance also suggests saturation mechanisms for zonal flows. Many works on zonal flow

generation[1, 2, 11, 12] exist, but the question of how zonal flows saturate, absent frictional drag, remains open. Though sometimes mentioned in this context, tertiary instability is *not* effective for most cases of ZF saturation as it is strongly suppressed by magnetic shear. Indeed, in simulation studies, onset of tertiary instability requires an *artificial* increase in the ZF shearing rate[13] so as to overcome the stabilizing effects of magnetic shear. Ion temperature gradients can provide an extra source of free energy to drive the tertiary mode, in addition to flow shear. However, such a contribution to the growth rate of the tertiary mode is of order $O(k^2\rho_i^2)$, and thus does not qualitatively alter tertiary stability[14]. Tertiary instability of ZF may occur in flat-q regimes[15] with zero magnetic shear. Even there, the key question of just how much turbulent mixing and flow damping result remains to be addressed.

In this work, we discuss the role of wave–flow resonance in zonal flow dynamics. Specifically, we investigate whether the conventional shear suppression rules still hold true when wave–flow resonance is considered. In addition, we study how resonance enters zonal flow regulation. In particular, we seek to answer the following questions:

(1) How do zonal flows saturate in the frictionless regime? What determines the stationary flow scale? To what degree is the often-quoted gyro-Bohm scaling broken?

(2) How do we incorporate the resonance effect in a predator–prey model? How is this new model different from previous ones?

We find that flow shear can destabilize the drift wave turbulence through the resonance. This *contradicts* the conventional wisdom that the flow shear always suppresses turbulence. Resonance between drift wave and plasma flow suppresses the instability by wave absorption. Increasing the flow shear, with fixed flow magnitude, can weaken the resonance. Consequentially, the flow shear increment actually *destabilizes* the drift wave turbulence. This suggests that the flow shear can affect the stability via resonance in a way opposite to what the conventional shear suppression models predict. Thus, wave-flow resonance is an important factor to be considered when studying shear flow effects on stability, and on quasilinear fluxes that transport particles, vorticity, and momentum.

We study drift–ZF turbulence with special focus on the frictionless regime where the flow drag $\to 0$. Note that the DW drive–which can depend on electron collisionality–is not affected by the distinction between frictional and frictionless ion regimes, since frictional

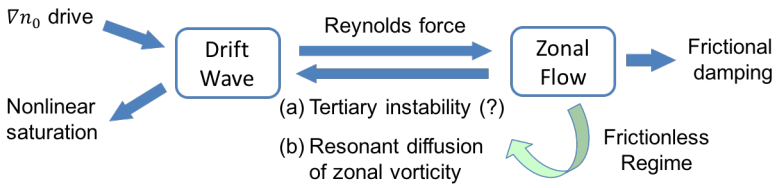

FIG. 1: Frictionless zonal flow saturation by (a) tertiary instability and (b) resonant vorticity diffusion.

damping of drift *waves* is weak. Many works on ZF generation[1, 2] exist, but the question of how ZF saturates, absent frictional drag, remains open. *We show that turbulent mixing of zonal vorticity by drift waves in the presence of ZF saturates secondary flows for near-marginal turbulence* (with low to zero frictional drag), *and thus is effective at regulating the Dimits up-shift regime.* The Dimits regime[1, 16] is that of a frictionless DW–ZF system close to the linear instability threshold, where nearly all the energy of the system is coupled to ZF, so that the residual transport and turbulence are weak, though finite. This induces an up-shift in the onset of the turbulent fluxes when plotted vs ∇T. Turbulent vorticity mixing is fundamentally different from viscous flow damping. Turbulent vorticity mixing conserves total potential enstrophy (PE) between the mean field–i.e., the zonal component–and fluctuations. In contrast, the flow viscosity dissipates both the ZF and (DW flow) fluctuations, and so is an energy sink for all. Fig. 1 illustrates the paradigm shift from the hypothetical saturation induced by tertiary instability to the saturation by vorticity mixing.

The ZF saturation mechanism induced by resonant vorticity mixing is incorporated as a nonlinear self-regulating effect in an extended predator-prey model[3, 4]. Stationary turbulence and flow states are calculated and compared in the frictionless, weakly frictional, and strongly frictional regimes. In the frictionless regime, the results are different from the conventionally quoted scalings derived for frictional regimes.

Turbulent vorticity mixing is driven by resonance between drift wave and zonal flow. It is analogous to Landau damping absorption of plasmons during collapse of Langmuir turbulence[17, 18]. In the latter case, plasmon Landau damping arrests collapse, leaving an "empty cavity", without its "filling" of Langmuir wave pressure. Table I compares these two processes. Both zonal flow formation and Langmuir collapse (i.e., the formation of caviton) result from modulational instability, and they both saturate in the collisionless regime. Moreover, both Landau damping and vorticity mixing conserve energy (or potential

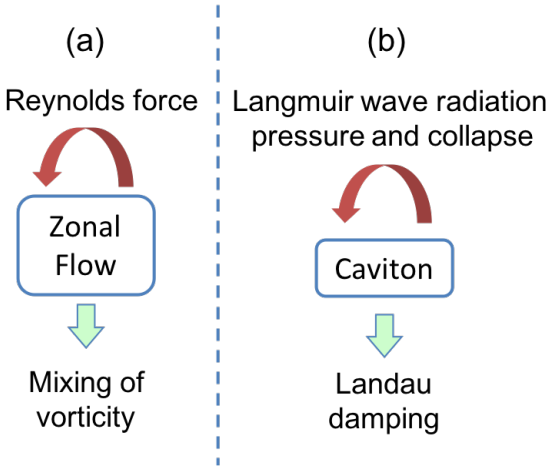

FIG. 2: Comparison of the generation and frictionless dissipation of (a) zonal flow and (b) caviton.

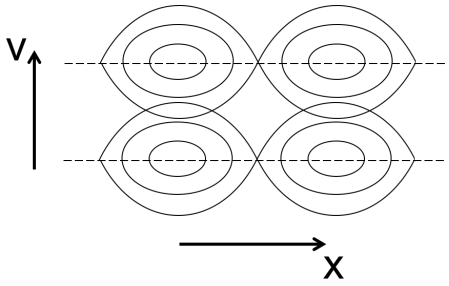

FIG. 3: Overlapping islands in phase space. The dashed lines represent resonant surfaces.

enstrophy, in the case of vorticity mixing). The key difference between the two is the detail of the resonance. The resonance considered here is between drift wave phase velocity and flow velocity, while conventional Landau resonance considers the resonance between phase velocity and particle velocity. Landau resonance defines a series of resonant surfaces in (x, v) phase space. When the islands around adjacent surfaces overlap, the trajectory of a particle becomes chaotic, leading to mixing of phase space density (Fig. 3). As a result, the particle PDF (probability density function) evolves stochastically, i.e., as by a Fokker–Planck equation in velocity. In contrast, resonant diffusion mixes vorticity in real space. The diffusive scattering of zonal vorticity profile is resonant. Therefore, irreversibility results from stochastic vorticity trajectories due to overlapping islands in real space, i.e., the (x, y) space.

The rest of this paper is organized as follows. Sec. II presents the wave-flow resonance effect on stability, specifically how the flow magnitude and flow shear affect the stability via resonance. Sec. III discusses how zonal flow saturation in the frictionless regime is regulated

TABLE I: Comparison and contrast of Landau damping effects on cavity collapse during Langmuir turbulence collapse and resonance effects on frictionless zonal flow (ZF) saturation.

	Langmuir turbulence collapse	Frictionless ZF saturation
Primary player	Plasmon-Langmuir wave	Drift wave turbulence
Secondary player	Ion-acoustic wave (caviton)	Zonal flow
Free energy source	Langmuir turbulence driver	∇n, ∇T drive
Final state	Nearly empty cavity	Saturated zonal flow and residual turbulence
Resonance	Landau damping	$\omega_k - k_y\langle v_y\rangle$ absorption
Other damping effects	Ion-acoustic radiation	Wave packet trapping

by the resonance. Sec. IV summarizes and discusses the main results of this paper.

II. WAVE-FLOW RESONANCE EFFECT ON STABILITY

Shear is not the only flow property that controls the stability of turbulence. We reconsider the shear suppression models by incorporating the the effects of resonance. Resonance between drift wave and flow stabilizes the turbulence via wave absorption. The flow shear weakens the resonance, and thus actually enhances the turbulence. Also, we show that the flow magnitude enhances the resonance, and thus, stabilizes the drift wave. The flow magnitude (V_{max}) is defined as the maximum flow velocity in the electron drift direction. Increasing V_{max} reduces the value of $\omega_k - kV_{max}$, and thus enhances the resonance.

We study the Hasegawa–Wakatani drift wave system in slab geometry with a mean perpendicular flow $\langle v_y\rangle$ varying in the $\hat{x}$ direction:

$$\left(\frac{d}{dt} + \tilde{\mathbf{v}}_E \cdot \nabla\right)\tilde{n} + \tilde{v}_x \frac{\nabla n_0}{n_0} = D_\parallel \nabla_\parallel^2 (\tilde{n} - \tilde{\phi}) + D_c \nabla^2 \tilde{n}, \tag{1}$$

$$\left(\frac{d}{dt} + \tilde{\mathbf{v}}_E \cdot \nabla\right)\tilde{\rho} + \tilde{v}_x \langle\rho\rangle' = D_\parallel \nabla_\parallel^2 (\tilde{n} - \tilde{\phi}) + \chi_c \nabla^2 \tilde{\rho}, \tag{2}$$

where we define $D_\parallel \equiv v_{The}^2/\nu_{ei}$ and $d/dt \equiv \partial_t + \langle v_y\rangle\partial_y$. ν_{ei} is the frequency of electron–ion collision and v_{The} is the electron thermal speed. We have normalized electric potential fluctuation as $\tilde{\phi} \equiv e\delta\phi/T_e$ and density fluctuation as $\tilde{n} \equiv \delta n/n_0$, where n_0 is the equilibrium density. The magnetic field is in the $\hat{z}$ direction, and both n_0 and $\langle v_y\rangle$ vary only in $\hat{x}$ direction. The vorticity fluctuation is $\tilde{\rho} \equiv \rho_s c_s \nabla_\perp^2 \tilde{\phi}$ where ρ_s is the ion Larmor radius at

electron temperature and c_s is the ion sound speed, and the zonal vorticity is $\langle\rho\rangle \equiv \langle v_y\rangle'$. $\tilde{\mathbf{v}}_E \equiv c_s\hat{\mathbf{z}}\times\nabla\tilde{\phi}$ is the $E\times B$ velocity fluctuation. D_c and χ_c are the collisional particle diffusivity and vorticity diffusivity (i.e., viscosity). Drift wave is the dominant instability population, because the vorticity gradient drive is quantitatively weaker than the ∇n_0 drive, i.e. $k_y\rho_s^2\langle v_y\rangle''/\omega_{*e} \ll 1$ where $\omega_{*e} \equiv k_y\rho_s c_s/L_n$ is the electron drift frequency and $L_n \equiv n_0/|dn_0/dx|$ is the density gradient scale.

In the following subsections, we show how conventional shear suppression models fail in the presence of strong wave–flow resonance.

A. Resonance Effects on Stability

Wave-flow resonance stabilizes drift waves through wave absorption. The instability is linked to the mode scale L_m (defined by Eq. (5)). The key resonance, here, is between the phase velocity of drift waves and the fluid velocity of plasma, i.e. $\omega_k - k_y\langle v_y\rangle$. Due to the resonance effect, the eigenmode peaks around the position where $|\omega_k - k_y\langle v_y\rangle|$ is a minimum. When the resonance becomes stronger, the scale of the eigenmode decreases. The mode scale is effectively the wavelength in the $\hat{x}$ direction, i.e. $k_x\rho_s \sim L_m^{-1}\rho_s$. Hence, the resonance regulates the turbulent fluxes by varying the mode scale.

We can write the fluctuating quantities in Eq. (1)–(2) as Fourier components in the $\hat{y}$ and parallel ($\hat{z}$) directions, while retaining the amplitude variation in the $\hat{x}$ direction, i.e.

$$\tilde{\phi}(x,y,z,t) = \sum_{k_y,k_\parallel} \phi(x) e^{i\left(k_y y + k_\parallel z - \Omega_k t\right)},$$

$$\tilde{n}(x,y,z,t) = \sum_{k_y,k_\parallel} n(x) e^{i\left(k_y y + k_\parallel z - \Omega_k t\right)}.$$

The complex frequency Ω_k consists of a real frequency and a growth rate, i.e. $\Omega_k = \omega_k + i\gamma_k$. Electrons are weakly non-adiabatic, i.e. $\tilde{n} = (1-i\delta)\tilde{\phi}$ with $\delta \ll 1$. The nonadiabatic electron response δ is determined by the frequency shift $\delta = (\omega_{*e} - \omega_k + k_y\langle v_y\rangle)/(k_\parallel^2 D_\parallel) \ll 1$, given that the adiabatic factor is $k_\parallel^2 D_\parallel/\omega_{*e} \gg 1$. The eigenmode equation for $\phi(x)$ is then

$$\left(\omega_k - k_y\langle v_y\rangle + i\gamma_k\right)\rho_s^2\partial_x^2\phi = \left[\left(1 + k_y^2\rho_s^2 - i\delta\right)\left(\omega_k - k_y\langle v_y\rangle + i\gamma_k\right) - \omega_{*e} - k_y\rho_s^2\langle v_y\rangle''\right]\phi, \quad (3)$$

where the collisional viscosity χ_c has been neglected. Multiplying both sides of Eq.(3) by ϕ^*, and integrating over the $\hat{x}$ direction, we obtain

$$\left(\omega_k - k_y\langle v_y\rangle + i\gamma_k\right) L_m^{-2}\rho_s^2 + \left[\left(1 + k_y^2\rho_s^2 - i\delta\right)\left(\omega_k - k_y\langle v_y\rangle + i\gamma_k\right) - \omega_{*e}\right] = 0 \tag{4}$$

where the mode scale L_m is defined by

$$L_m^{-2}\rho_s^2 \equiv \frac{\rho_s^2 \int_0^{L_x} dx|\partial_x\phi|^2}{\int_0^{L_x} dx|\phi|^2}. \tag{5}$$

Here, we have used the boundary condition $\phi(0) = \phi(L_x) = 0$. In addition, the vorticity gradient term is ignored in Eq.(4), because it is quantitatively negligible as compared to ω_{*e}.

The Doppler shifted frequency and the growth rate are obtained from Eq. (4)

$$\omega_k \cong \frac{\omega_{*e}}{1 + k_y^2\rho_s^2 + L_m^{-2}\rho_s^2}, \tag{6}$$

$$\gamma_k \cong \frac{\omega_{*e}^2}{k_\parallel^2 D_\parallel} \frac{k_y^2\rho_s^2 + L_m^{-2}\rho_s^2}{(1 + k_y^2\rho_s^2 + L_m^{-2}\rho_s^2)^3}. \tag{7}$$

When resonance becomes stronger, i.e. $|\omega_k - k_y\langle v_y\rangle|_{\min}$ decreases, the eigenmode becomes narrower (mode scale L_m/ρ_s decreases), and thus the growth rate decreases. Therefore, stronger resonance stabilizes the drift wave.

B. Effect of Flow Magnitude on Stability

Increasing the flow magnitude enhances resonance, thus stabilizes the drift wave. We consider the regime where $0 < |\omega_k - k_y\langle v_y\rangle|_{\min} \ll \omega_{*e}$. Here, the resonance is stronger, but there is no singularity in the eigenmode equation. As $\langle v_y\rangle$ increases, resonance is enhanced. Therefore, increasing the flow *magnitude* suppresses instability.

In order to illustrate the effect of flow on the resonance, and thus on stability, we numerically solve the eigenmode equation Eq. (3) for wave frequency ω_k, growth rate γ_k, and eigenmode profile $\phi(x)$. The chosen parameters are a proxy for realistic CSDX parameters, which are $L_x = 6$ cm, $\rho_s = 1.2$ cm, $L_n = 2$ cm, $k_y\rho_s = \pi/L_x$. Dirichlet boundary conditions are used, which are $\phi(0) = \phi(L_x) = 0$. The adiabatic factor is $k_\parallel^2 D_\parallel/\omega_{*e} = 3$, so electrons

are nearly adiabatic with $\delta \cong 1/3$. We use the hyperbolic tangent function to describe the flow profile, which is

$$\langle v_y \rangle = V_{max} \tanh \frac{x - 0.5L_x}{L_V}. \tag{8}$$

Here, the maximum flow shear is given by V_{max}/L_V. This allows us to vary either the flow magnitude or the flow shear, while keeping the other fixed.

As the flow magnitude increases and the flow shear remains constant, the resonance becomes stronger (Fig. 6, left panel). Hence, the mode peak moves closer to the position with the minimum $|\omega_k - k_y \langle v_y \rangle|$, which is at $x = L_x$ (Fig. 5). As a result, instability is suppressed (Fig. 6, right panel).

C. Effect of Flow Shear on Stability

Flow shear weakly destabilizes the drift wave by weakening the resonance. As a result, the eigenmode profile is flattened (Fig. 7). This increases the mode scale L_m/ρ_s (Fig. 8, left panel). Hence, the drift wave is destabilized by the flow shear (Fig. 8, right panel).

Note that the increment in growth rate is not due to enhanced KH instability, because KH drive is quantitatively negligible as compared to drift wave drive here.

III. FRICTIONLESS ZF SATURATION BY RESONANT PV MIXING

In this section, we show that resonant scattering of the zonal vorticity can saturate secondary flows in the frictionless regime. This process is distinct from the tertiary mechanism. This shift in paradigm is illustrated by the diagram in Fig. 1. The resonant vorticity diffusion can saturate flows in both marginal and strong turbulence regimes. The stationary flow results from the balance between the residual vorticity flux and the resonant scattering effect. Since both of them scale with the turbulence intensity, the stationary flow is then independent of turbulence strength to leading order. Therefore, this saturation mechanism is effective in the Dimits up-shift regime, where turbulence is marginally unstable. We calculate the stationary zonal flow shear and scale directly from analysis, and determine the degree of gyro-Bohm breaking resulting from strong zonal flow shear.

This saturation mechanism is incorporated into a extended 0D predator–prey model. The flow state and turbulence level are calculated for frictionless, weakly frictional, and strongly

frictional regimes, and compared to previous results. Also, we use drift wave turbulence as an example case to calculate the saturated flow state in the frictionless regime. Study for the 0D model lends considerable insight by enabling calculation of flow scales, and flow and turbulence states (i.e., fixed points). However, a 1D model is necessary to study the spatiotemporal evolution in physical systems, such as staircase formation and avalanches[19, 20].

A. Drift Wave–Zonal Flow System in the Resonant PV Mixing Framework

The generation and saturation of zonal flows by drift waves are described by PV (potential vorticity) mixing. The fluctuating PV is defined as $\tilde{q} \equiv \tilde{n} - \tilde{\rho}$, and the zonal PV is $\langle q \rangle \equiv \langle n \rangle - \langle \rho \rangle$. Hence, the evolution equation for fluctuating PV can be obtained by subtracting Eq. (2) from Eq. (1), yielding

$$\left(\frac{d}{dt} + \tilde{\mathbf{v}}_E \cdot \nabla \right) \tilde{q} + \tilde{v}_x \frac{\partial}{\partial x} \langle q \rangle = D_{q,c} \nabla^2 \tilde{q}. \tag{9}$$

Here, $D_{q,c} \sim (D_c + \chi_c)/2$ is the collisional diffusivity of PV. In multiplying both sides of Eq. (9) by $\tilde{q}$, we obtain the potential enstrophy (PE)–i.e., $\Omega \equiv \langle \tilde{q}^2 \rangle / 2$–equation[21, 22]:

$$\frac{\partial}{\partial t} \Omega = -\frac{\partial}{\partial x} \frac{\langle \tilde{v}_x \tilde{q}^2 \rangle}{2} - \langle \tilde{v}_x \tilde{q} \rangle \frac{\partial}{\partial x} \langle q \rangle - \varepsilon_c \Omega^{3/2} + \gamma_L \Omega. \tag{10}$$

The turbulent PE flux is due to nonlinear spreading, and can be approximated as a diffusive flux, i.e., $\langle \tilde{v}_x \tilde{q}^2 \rangle / 2 \sim -D_\Omega \partial_x \Omega$[21]. The nonlinear PE dissipation $\varepsilon_c \Omega^{3/2}$ represents the forward cascade (to dissipation) of PE. γ_L is the characteristic linear growth rate of drift waves, which drives the turbulence and thus produces PE. The coupling of PV flux and zonal PV profile gradient conserves PE between mean field and fluctuations.

The equations for mean-field density and zonal vorticity are

$$\frac{\partial}{\partial t} \langle n \rangle = -\frac{\partial}{\partial x} \langle \tilde{v}_x \tilde{n} \rangle + D_c \nabla^2 \langle n \rangle, \tag{11}$$

$$\frac{\partial}{\partial t} \langle \rho \rangle = -\frac{\partial}{\partial x} \langle \tilde{v}_x \tilde{\rho} \rangle - \mu_c \langle \rho \rangle - \mu_{NL} \langle \rho \rangle + \chi_c \nabla^2 \langle \rho \rangle. \tag{12}$$

μ_c is frictional drag coefficient. The nonlinear flow damping rate μ_{NL} depends on $\langle \rho \rangle$, and is

set by tertiary modes, e.g. Kelvin–Helmholtz instability of zonal flows. In reality, the onset of such tertiary modes requires the ZF shear to exceed a threshold[13], in order to overcome the damping of magnetic shear. Onset of tertiary instability can be included in reduced models, if needed. However, here we neglect it, because the relevance of such tertiary modes to ZF saturation in confinement devices is negligible.

To close the system, we need to calculate the turbulence-driven fluxes. The quasilinear PV flux is diffusive, i.e.,

$$\langle \tilde{v}_x \tilde{q} \rangle = -D_{q,turb} \frac{\partial}{\partial x} \langle q \rangle, \tag{13}$$

which is obtained from Eq. (9), neglecting collisional diffusion. Here, the turbulent diffusivity of PV has a resonant part and a non-resonant part, i.e., $D_{q,turb} = D_q^{\text{res}} + D_q^{\text{non-res}}$.

The resonant diffusivity of PV is set by the resonance between phase velocity of drift wave and the local ZF profile, which yields

$$D_q^{\text{res}} = \sum_k |\tilde{v}_{x,k}|^2 \pi \delta(\omega_k - k_y \langle v_y \rangle), \tag{14}$$

where $\tilde{v}_{x,k}$ is the fluctuating velocity in the radial direction and ω_k is the drift wave frequency. The resonant scattering here has a characteristic spectral autocorrelation time scale $\tau_{ck} \sim |\Delta(\omega_k - k_y \langle v_y \rangle)|^{-1} \sim \{|(v_{g,y} - v_{ph,y})\Delta k_y| + |v_{g,x} \Delta k_x|\}^{-1}$, where we have used $\langle v_y \rangle \cong \omega_k / k_y = v_{ph,y}$. The resonance is between drift waves and the instantaneous ZF profile. Thus, this autocorrelation time is shorter than the time scale of ZF evolution, i.e., $\tau_{ck} \ll \tau_{ZF}$, consistent with ZF evolution by turbulent PV mixing. The correlation time τ_{ck} is shorter as compared to the 1D case, where the spectral width is associated with the mismatch between group velocity and phase velocity, i.e., $\tau_{ck} \sim |(v_g - v_{ph})\Delta k|^{-1}$, only. As a result, the resonant diffusivity is $D_q^{\text{res}} = \sum_k k_y^2 \rho_s^2 c_s^2 |\phi_k|^2 \tau_{ck}$.

The non-resonant diffusivity can be obtained by quasilinear theory, and is

$$D_q^{\text{non-res}} = \sum_{\omega_k \neq k_y \langle v_y \rangle} k_y^2 \rho_s^2 c_s^2 |\phi_k|^2 \frac{|\gamma_k|}{|\omega_k - k_y \langle v_y \rangle|^2}. \tag{15}$$

γ_k is the linear growth rate of drift waves. In marginally stable turbulence, γ_k should be replaced by the nonlinear decorrelation rate of turbulence, i.e., $\Delta\omega N_k / N_0$ where $N_k \sim |\phi_k|^2 / \omega_k$ is the wave action density. As a consequence, in marginally stable turbulence, the

non-resonant diffusivity is

$$D_q^{\text{non-res}} = \sum_{\omega_k \neq k_y \langle v_y \rangle} k_y^2 \rho_s^2 c_s^2 \frac{|\Delta\omega|}{I_0} \frac{|\phi_k|^2 |\phi_k|^2}{|\omega_k - k_y \langle v_y \rangle|^2}, \tag{16}$$

where $I_0 \equiv \sum_k |\phi_k|^2$. This is analogous to wave–particle scattering due to higher order Landau resonance[23] in Vlasov plasmas. The Doppler shifted frequency and the growth rate of the drift wave are given by Eq. (6) and (7). Both of them depend upon the eigenmode scale in radial direction, which is $L_m \equiv \langle k_x^2 \rangle^{-1/2}$. Thus, the non-resonant diffusivity depends on the mode scale, which yields

$$D_q^{\text{non-res}} \sim \sum_{\omega_k \neq k_y \langle v_y \rangle} \frac{k_y^2 \rho_s^2 c_s^2}{k_\parallel^2 D_\parallel} \frac{k_y^2 \rho_s^2 + L_m^{-2} \rho_s^2}{1 + k_y^2 \rho_s^2 + L_m^{-2} \rho_s^2} |\phi_k|^2. \tag{17}$$

The mode scale does not affect the turbulent diffusivity significantly. This follows since for drift wave scaling where $k_y \rho_s \sim 1$, the factor involving the mode scale does not vary strongly (with that scale) while it ranges from 0.5 to 1. The non-resonant diffusivity is negligible in comparison to the resonant diffusivity, because $D_q^{\text{non-res}} \sim (k_\parallel^2 D_\parallel)^{-1}$ and $k_\parallel^2 D_\parallel \gg \tau_{ck}^{-1}$ for near–adiabatic electrons. Therefore, the mixing of PV is primarily *resonant*.

The turbulent particle flux driven by drift wave turbulence in the adiabatic regime is diffusive, i.e.,

$$\langle \tilde{v}_x \tilde{n} \rangle = -D_{n,\text{turb}} \frac{\partial}{\partial x} \langle n \rangle, \tag{18}$$

where

$$D_{n,\text{turb}} = \sum_k \frac{k_y^2 \rho_s^2 c_s^2}{k_\parallel^2 D_\parallel} \frac{k_y^2 \rho_s^2 + L_m^{-2} \rho_s^2}{1 + k_y^2 \rho_s^2 + L_m^{-2} \rho_s^2} |\phi_k|^2. \tag{19}$$

We can then obtain the vorticity flux by subtracting the PV flux from the particle flux, i.e., $\langle \tilde{v}_x \tilde{\rho} \rangle = \langle \tilde{v}_x \tilde{n} \rangle - \langle \tilde{v}_x \tilde{q} \rangle$, which is

$$\langle \tilde{v}_x \tilde{\rho} \rangle = -(D_{n,\text{turb}} - D_q^{\text{res}}) \frac{\partial}{\partial x} \langle n \rangle - D_q^{\text{res}} \frac{\partial}{\partial x} \langle \rho \rangle. \tag{20}$$

Here, the last term is the flux induced by resonant diffusion. The non-diffusive component forms a *residual vorticity flux*, i.e., $\Gamma_\rho^{Res} = -(D_{n,\text{turb}} - D_q^{\text{res}}) \partial_x \langle n \rangle$. Γ_ρ^{Res} is driven by drift wave turbulence, so it is proportional to the density gradient. As discussed in Ref. [1], Γ_ρ^{Res} drives zonal flows against diffusive vorticity mixing. The gradient of Γ_ρ^{Res} can accelerate zonal flows

from rest. Note that this mean field calculation of the vorticity flux is technically applicable to the stationary state, while modulational instability analysis is limited to the stage of ZF growth.

We then arrive at the DW–ZF system including resonant PV mixing, which is

$$\frac{\partial}{\partial t}\langle n\rangle = \frac{\partial}{\partial x} D_{n,\mathrm{turb}} \frac{\partial}{\partial x}\langle n\rangle + D_c \nabla^2 \langle n\rangle, \tag{21}$$

$$\frac{\partial}{\partial t}\langle \rho\rangle = \frac{\partial}{\partial x}\left[(D_{n,\mathrm{turb}} - D_q^{\mathrm{res}}) \frac{\partial}{\partial x}\langle n\rangle + D_q^{\mathrm{res}} \frac{\partial}{\partial x}\langle \rho\rangle \right] - \mu_c \langle \rho\rangle - \mu_{NL}\langle \rho\rangle + \chi_c \nabla^2 \langle \rho\rangle, \tag{22}$$

$$\frac{\partial}{\partial t}\Omega = D_\Omega \frac{\partial^2}{\partial x^2}\Omega + D_q^{\mathrm{res}} \left[\frac{\partial}{\partial x}(\langle n\rangle - \langle \rho\rangle) \right]^2 - \varepsilon_c \Omega^{3/2} + \gamma_L \Omega. \tag{23}$$

This system consists of the equations for mean-field density (Eq. (21)), zonal vorticity (Eq. (22)), and fluctuation PE (Eq. (23)). Initially produced by linear drift wave instability, the PE of this system is conserved up to frictional dissipation and nonlinear turbulent saturation, which transfer PE to small scales. The evolution of total PE is given by

$$\frac{\partial}{\partial t}\int dx \left[\Omega + \frac{(\langle n\rangle - \langle \rho\rangle)^2}{2} \right] = \int dx \left[\gamma_L \Omega - \varepsilon_c \Omega^{3/2} - D_{q,c} |\nabla(\langle n\rangle - \langle \rho\rangle)|^2 - \mu_c \langle \rho\rangle^2 - \mu_{NL}\langle \rho\rangle^2 \right]. \tag{24}$$

The collisional diffusion of zonal PV (the term with $D_{q,c}$ in Eq. (24)) is a sink. In contrast, the turbulent PV diffusion conserves PE between mean field and fluctuations.

B. Frictionless ZF Saturation via Resonant PV Diffusion

As demonstrated by Ref. [24, 25], vorticity flux is identical to the Reynolds force, and thus drives the zonal flow. The residual vorticity flux excites the zonal flow, and thus the resonant diffusion is the only damping for zonal flows in the frictionless limit–i.e., $\mu_c, \chi_c, \mu_{NL} \to 0$. By multiplying Eq. (22) by $\langle \rho\rangle$, we obtain the net production of mean flow enstrophy in the frictionless limit, which is

$$\frac{\partial}{\partial t}\int dx \frac{\langle \rho\rangle^2}{2} = \int dx \left[-(D_{n,\mathrm{turb}} - D_q^{\mathrm{res}}) \frac{\partial \langle n\rangle}{\partial x} \frac{\partial \langle \rho\rangle}{\partial x} - D_q^{\mathrm{res}} \left(\frac{\partial \langle \rho\rangle}{\partial x} \right)^2 \right]. \tag{25}$$

Hence, we see resonant diffusion of zonal vorticity saturates zonal flows in the frictionless regime–i.e., its contribution to $\partial_t \int dx \langle \rho\rangle^2$ is negative definite.

The zonal vorticity profile is stationary when the net flow production is zero, i.e., $\partial_t \int dx \langle\rho\rangle^2 = 0$. Therefore, in the frictionless regime, the stationary vorticity profile is determined by the balance between residual vorticity flux and the resonant vorticity diffusion (i.e., so $\langle\tilde{v}_x\tilde{\rho}\rangle = 0$) which implies

$$\langle v_y\rangle'' \sim -\frac{c_s}{\rho_s L_n}\left(1 - \frac{1}{\tau_{ck}k_\parallel^2 D_\parallel}\frac{k_y^2\rho_s^2 + L_m^{-2}\rho_s^2}{1 + k_y^2\rho_s^2 + L_m^{-2}\rho_s^2}\right). \tag{26}$$

In the relevant limit of near-adiabatic electrons, i.e., $\tau_{ck}k_\parallel^2 D_\parallel \gg 1$, the zonal flow scale is

$$L_{ZF} \sim \left(\frac{\langle v_y\rangle}{c_s}\right)^{1/2}\sqrt{\rho_s L_n}. \tag{27}$$

Only a fraction of turbulence energy is coupled to zonal flows. Thus, the flow magnitude is obtained using mixing length estimation for the turbulence energy, and a coupling fraction f:

$$\frac{\langle v_y\rangle^2}{c_s^2} \sim f\frac{l_{mix}^2}{L_n^2}. \tag{28}$$

Here, $0 < f < 1$ is the fraction of turbulence energy coupled to the zonal flow. Note that f and the mixing length are as yet unspecified. The flow scale follows as $L_{ZF} \sim f^{1/4}\sqrt{\rho_s l_{mix}}$, which depends only weakly on f. Clearly, the mixing length is much larger than the microscale (ρ_s) and can be as large as an extended cell ($\sim L_n$), i.e., $\rho_s \ll l_{mix} \leq L_n$. Indeed, $l_{mix} \sim L_n$ is the appropriate "base state" scale, absent zonal flows. Thus, L_{ZF} necessarily lies between the microscale (ρ_s) and the mixing scale (l_{mix}). The questions are to determine the relative weighting of l_{mix} and ρ_s, and to account for shear modification of l_{mix}.

To determine l_{mix}, note that the base state mixing length is reduced by zonal flow shearing. This yields

$$l_{mix}^2 \sim \frac{l_0^2}{1 + (\langle v_y\rangle'\tau_c)^2}, \tag{29}$$

where l_0 is the mixing length for zero flow shear. In the case of drift wave turbulence, we have $l_0 \sim L_n$ for extended cells absent flow shear.

For weak or modest zonal flow shear, the decorrelation time is the eddy turnover time. The eddy size is set by the mixing length and the eddy turning speed is set by the mean square root of the velocity fluctuations. Then, we obtain $\tau_c \sim \varepsilon^{-1/2} \sim l_{mix}/\langle\tilde{v}^2\rangle^{1/2}$. The

mixing length model yields $\langle \tilde{v}^2 \rangle / c_s^2 \sim (1-f) l_{mix}^2 / L_n^2$. Thus, the mixing length is $l_{mix}^2 \sim (1-f) l_0^2 \Big/ \left(\frac{|\langle v_y \rangle|}{c_s} \frac{L_n}{L_{ZF}} \right)^2$. As a result, the zonal flow scale is $L_{ZF} \sim f^{1/6} (1-f)^{1/6} \rho_s^{2/3} l_0^{1/3}$. The zonal flow shear is then $|\langle v_y \rangle'| \sim f^{1/6} (1-f)^{1/6} \frac{c_s}{L_n} \left(\frac{l_0}{\rho_s} \right)^{1/3}$.

For strong zonal flow shear, i.e., $\langle v_y \rangle' \gg$ eddy turnover rate, the decorrelation time is set by $\tau_c \sim (\langle v_y \rangle'^2 k_r^2 D)^{-1/3}$, i.e., the scale set by the well known interaction of shearing and radial scattering[26]. Due to the strong zonal flow shear, the turbulent diffusivity is resonant, so $D \sim \sum_k |\tilde{v}_r|^2 \delta(\omega_k - k_\theta \langle v_y \rangle)$. The resonance time scale is controlled by the shearing rate, which yields $\delta(\omega_k - k_\theta \langle v_y \rangle) \sim |\langle v_y \rangle'|^{-1}$. Hence, the diffusivity becomes $D \sim (1-f)(c_s^2 / |\langle v_y \rangle'|)(l_{mix}^2 / L_n^2)$. The mixing length is $l_{mix}^2 \sim (1-f)^{2/3} l_0^2 \Big/ \left(\frac{|\langle v_y \rangle|}{c_s} \frac{L_n}{L_{ZF}} \right)^{4/3}$. The zonal flow scale is $L_{ZF} \sim f^{3/16} (1-f)^{1/8} \rho_s^{5/8} l_0^{3/8}$. The zonal flow shear is then $|\langle v_y \rangle'| \sim f^{3/16} (1-f)^{1/8} \frac{c_s}{L_n} \left(\frac{l_0}{\rho_s} \right)^{3/8}$. Here, the flow shear is larger, and the flow scale is larger. This follows because $|\langle v_y \rangle'| \sim |\langle v_y \rangle| / L_{ZF}$ and both $|\langle v_y \rangle| / c_s$ and L_{ZF} increase with the underlying drive scale (l_{mix}). Nevertheless, the flow shear calculated here is close to that calculated for the weak shear case. Hence, in both cases, the flow shear are similar.

In either case, the factors f and $1-f$ enter with small exponents. Thus, the zonal flow emerges as mesoscopic, but weighted somewhat more strongly toward microscale (ρ_s) than macroscale (l_0). Note that while the mesoscopic zonal flow scale, i.e., $\rho_s < L_{ZF} < L_n$ and $L_{ZF} \sim \sqrt{\rho_s L_n}$ in particular, is frequently assumed, here they are determined by the analysis. The zonal flow shears in both cases are similar and robust. Even for the weak shear case, the calculated zonal flow shear is significant. Hence, the case of strong zonal flow shear–and thus flow resonance–is likely to be most relevant to the frictionless DW–ZF system discussed here. Note that we have calculated the zonal flow scale and shear self-consistently by considering the shearing feedback on mixing length. Externally driven flows may enhance the flow shearing, and thus reduces the mixing scale.

This mesoscopic zonal flow appears as a limiting case with near-adiabatic electrons (i.e., $\tau_{ck} k_\parallel^2 D_\parallel \gg 1$). In this limit, zonal flow scale does not depend on wave-numbers ($k_y \rho_s$). When $\tau_{ck} k_\parallel^2 D_\parallel$ is comparable to unity, L_{ZF} is linked to the mode scale. In that case, the resonance between drift wave and zonal flow regulates the flow structure by modifying the local mode scale. Also, the flow structure is sensitive to wave-numbers due to the second term of Eq. (26). In the hydrodynamic limit (i.e., $\tau_{ck} k_\parallel^2 D_\parallel \ll 1$), the generation and saturation of zonal flows must be reconsidered. The drift wave model discussed here is not directly applicable

to the hydrodynamic case where convective cells, not drift waves, are generated.

The mixing length derived here allows us to calculate the scaling of turbulent diffusivity with $\rho_* \equiv \rho_s/L_n$. Following the mixing length model, the turbulent diffusivity scales as $D \sim l_{mix} v_*$, where $v_* \equiv \rho_s c_s/L_n$ is the electron drift velocity. Thus, we obtain $D \sim D_B l_{mix}/L_n$, where $D_B \sim \rho_s c_s$ is the Bohm diffusivity. When there is no zonal flow, the mixing length is the size of an extended cell, i.e., $l_{mix} \sim L_n$. This recovers the Bohm scaling, i.e., $D \sim D_B$. In the presence of zonal flow shear, the mixing length is larger than ρ_s, and thus gyro-Bohm scaling is a lower bound for turbulent diffusivity, i.e., $D > D_B \rho_*$. Hence, D lies between the gyro-Bohm and Bohm limits, i.e., $D \sim D_B \rho_*^\alpha$ where $0 < \alpha < 1$. The question is to determine α, i.e., the degree of gyro-Bohm breaking. The mixing length in the case of strong zonal flow shear is $l_{mix} \sim \rho_s^{1/4} l_0^{3/4} \sim \rho_s^{1/4} L_n^{3/4}$. This indicates that the scaling of turbulent diffusivity is closer to the Bohm regime, i.e., $D \sim D_B l_{mix}/L_n \sim D_B \rho_*^{1/4} (l_0/L_n)^{3/4} \sim D_B \rho_*^{1/4}$. Therefore, the zonal flow shear leads to a gyro-Bohm correction to the diffusivity which is initially Bohm, absent flow shear. As a result, the diffusivity lies somewhere between Bohm and gyro-Bohm, but weighted more toward Bohm. Note the zonal flow shear here is determined self-consistently by considering shearing feedback on mixing length. Externally driven flow shears are not restricted by this self-consistent feedback mechanism. Thus, the external flow shear could make the diffusivity weighted more toward gyro-Bohm, i.e., $D \sim D_B \rho_*^{1/4+\beta}$ where $\beta > 0$ is induced by external shear. External shear reduces the mixing scale through the shearing feedback. Also, increasing external power input may lead to the formation of transport barriers[15]. The barriers can then reduce the mixing scale and thus can make the diffusivity more gyro-Bohm.

C. Extended Predator–Prey Model

The frictionless saturation induced by resonant PV mixing can be incorporated in the predator–prey model of the DW–ZF system. In this subsection, we show the derivation of this new, 0D model and compare the results with previous models. Note that even though the 0D model studied here is sufficient to demonstrate the flow and turbulence states as well as the flow scale, a model with at least one spatial dimension is necessary to study the spatiotemporal *dynamics* of the system, such as the formation of transport barriers.

Eq. (25) shows that in the frictionless regime, the net production of zonal field enstrophy

is driven by the vorticity flux. Ignoring the evolution of $\langle n \rangle$, the total mean-field PE is related to the zonal vorticity through $V''^2 \sim \int dx \langle v_y \rangle'^2 / L_{ZF}^2 \equiv \int dx \langle \rho \rangle^2 / L_{ZF}^2$. The total fluctuation PE is $E \equiv \int dx \Omega$. Zonal flow is driven by the residual vorticity flux, but dissipated by the resonant scattering of zonal vorticity. Thus, the *net* mean-field PE is produced by $\langle \tilde{v}_x \tilde{\rho} \rangle V'' = \Gamma_\rho^{Res} V'' - D_q^{\rm res} V''^2 \sim \alpha_1 E |V''| - \alpha_2 V''^2 E$. Therefore, with frictional damping and nonlinear damping by tertiary instability included, the predator (flow) equation is

$$\frac{L_{ZF}^2}{2} \frac{dV''^2}{dt} = \alpha_1 |V''| E - \alpha_2 V''^2 E - \gamma_{NL} V''^2 - \mu_c V''^2. \tag{30}$$

The vorticity flux conserves enstrophy between zonal field and fluctuations. Thus, the residual vorticity flux forms a *sink* of the fluctuation PE and the resonant vorticity diffusion forms a *source*. As a consequence, the prey (turbulence) equation can be written as

$$\frac{dE}{dt} = -\alpha_1 |V''| E + \alpha_2 V''^2 E - \varepsilon_c E^{3/2} + \gamma_L E. \tag{31}$$

Here, baseline (i.e., without flow) nonlinear saturation of turbulence is through the forward cascade of PE. Ultimately, PE is dissipated by collisional diffusion at small scales. The linear growth of energy is due to the (linear) instability of fluctuations.

Eq. (30) and (31) form a new predator-prey model for the DW-ZF system. This model conserves PE and includes resonant PV mixing. The model is zero dimensional, because the quantities here have been integrated over space. Though the accuracy of this simplified 0D model is limited, we can use it to obtain useful insights. In this new model, the net flow production by turbulence consists of two terms, which are the turbulent production driven by residual stress and the dissipation induced by resonant diffusion.

Eq. (30) shows that in the frictionless regime, where the frictional drag $\mu_c \to 0$, the resonant vorticity diffusion saturates the zonal flow production, even without the nonlinear damping induced by tertiary instability. It should be stated that drift wave instability requires finite *electron* collisionality, while the frictional drag and collisional diffusion of particles and vorticity are both determined by *ion* collisionality and/or ion-neutral drag. Hence, flipping between frictional and frictionless regimes does not require a change in the drift wave drive.

The flow and energy states are set by the fixed points of the system, i.e. $dV''^2/dt =$

TABLE II: Flow states and turbulence states compared among regimes with different frictional damping rates. μ_c is the frictional drag coefficient, E is the turbulence energy (measured by fluctuation enstrophy), γ_L is the linear growth rate of turbulence, and α_1 and α_2 are coefficients in the predator–prey model resulting from residual vorticity flux and vorticity diffusion.

Regime	Frictionless	Weakly Frictional	Strongly Frictional
Frictional Damping Strength	$\mu_c \ll \alpha_2 E$	$\alpha_2 E \ll \mu_c \ll 4\gamma_L \alpha_1^2/\varepsilon_c^2$	$\mu_c \gg 4\gamma_L \alpha_1^2/\varepsilon_c^2$
Flow $\lvert V'' \rvert$	$\frac{\alpha_1}{\alpha_2}$	$\frac{\alpha_1 \gamma_L^2}{\mu_c \varepsilon_c^2}$	$\frac{\gamma_L}{\alpha_1}$
Turbulence Energy E	$\frac{\gamma_L^2}{\varepsilon_c^2}$	$\frac{\gamma_L^2}{\varepsilon_c^2}$	$\frac{\gamma_L \mu_c}{\alpha_1^2}$

$dE/dt = 0$. We ignore the nonlinear flow damping by tertiary instability, because it is irrelevant (usually). Therefore, the flow state can be obtained from Eq. (30), and is

$$|V''| = \frac{\alpha_1 E}{\alpha_2 E + \mu_c}. \tag{32}$$

We next discuss three regimes—the frictionless regime, the weakly frictional regime, and the strongly frictional regime—and compare results to those of previous models. In particular, we emphasize *what determines the turbulence level* and *what affects the flow* in near-marginal turbulence. The states of zonal vorticity and turbulence energy are summarized in Table II. In the frictionless regime, the turbulence energy level is set only by the linear instability growth rate and the nonlinear dissipation of PE. This differs from the strongly frictional regime, where the turbulence level is set by the frictional drag[3].

1. Frictionless regime

In the frictionless regime, the drag is negligible compared to the resonant diffusive scattering of vorticity, i.e. $\mu_c \ll \alpha_2 E$. The flow and turbulence states are given by

$$|V''| = \alpha_1/\alpha_2, \tag{33}$$

$$E = (\gamma_L/\varepsilon_c)^2. \tag{34}$$

The flow is determined, to leading order, by the balance between residual vorticity flux (α_1) and diffusive mixing of vorticity (α_2). The turbulence energy is basically determined by the balance between linear growth rate and dissipation rate of PE (ε_c).

In the frictionless regime, turbulence energy is (approximately) independent of the flow state. The turbulence energy is determined only by the linear instability drive and the nonlinear dissipation of PE. The dissipation rate tied to forward cascade of potential enstrophy is $\sim \varepsilon_c \Omega^{1/2} \sim \varepsilon_c E^{1/2}$. The turbulence state is then set by the balance between the linear growth rate and the nonlinear dissipation rate, i.e. $\gamma_L \sim \varepsilon_c E^{1/2}$, yielding $E \sim (\gamma_L/\varepsilon_c)^2$. When the linear drive is weak, i.e. $\gamma_L/\varepsilon_c < 1$, the turbulence becomes marginal, with $E \ll 1$. This is different from previous results, where turbulence energy is set by the frictional flow damping. In previous models, below the onset threshold for tertiary instability, the flow is dissipated only by frictional drag. The energy is coupled from turbulence to flow, which is a one-way coupling. Therefore, the fixed point is set by the balance between the frictional flow damping and energy coupling, i.e., $\alpha V E \sim \mu_c V$, where α is the coupling coefficient between flow and turbulence energy. As a result, the saturated turbulence energy $E \sim \mu_c/\alpha$.

In addition, the saturated flow does not depend on the *turbulence level*, to leading order. The balance between residual vorticity flux and the resonant vorticity diffusion sets the flow. In this balance, the turbulence intensity cancels out. This means there can be significant zonal flow, even when the turbulence is weak. Therefore, this new frictionless saturation mechanism, induced by resonant PV mixing, is effective for turbulence near marginality. In previous models, the flow is set by the difference between linear growth of turbulence and frictional flow damping[1]. Those models are not relevant to near-marginal turbulence, where $\gamma_L \to 0$.

2. Weakly frictional regime

When the drag exceeds the rate of turbulent diffusion, i.e. $\mu_c \gg \alpha_2 E$, the flow is linked to the turbulence strength, which is given by

$$|V''| = \alpha_1 E/\mu_c. \tag{35}$$

This follows because the flow is driven by turbulence, and collisions are the major source of flow damping. Thus, in the near marginal regime, both the turbulence and the flow becomes very weak, as the turbulence drive approaches zero.

The turbulence energy can be obtained from

$$\frac{\alpha_1^2 E}{\mu_c \gamma_L} + \frac{\varepsilon_c \sqrt{E}}{\gamma_L} - 1 = 0. \tag{36}$$

The exact solution is

$$E = \frac{\varepsilon_c^2 \mu_c^2}{2\alpha_1^4} \left[\sqrt{1 + \frac{4\gamma_L \alpha_1^2}{\varepsilon_c^2 \mu_c}} - 1 \right]. \tag{37}$$

Hence, in the weakly frictional regime, i.e. $\mu_c \ll 4\gamma_L \alpha_1^2/\varepsilon_c^2$, the turbulence energy is the same as in the frictionless case, while the flow is given by

$$|V''| = \frac{\alpha_1 \gamma_L^2}{\mu_c \varepsilon_c^2}. \tag{38}$$

We thus see that the weakly frictional regime is a hybrid of the frictionless and strongly frictional regimes. On one hand, the turbulence level is independent of flow damping, as for the frictionless regime. On the other hand, the flow depends on the turbulence level, meaning that when the turbulence is near marginal, the flow becomes very weak. This is because the turbulence driven flow production must be strong enough to overcome frictional damping, in order to drive a significant flow.

3. Strongly frictional regime

When the frictional flow damping is strong, i.e. in the strong frictional regime where $\mu_c \gg 4\gamma_L \alpha_1^2/\varepsilon_c^2$, the turbulence energy is set by the flow damping, which is given by

$$E = \gamma_L \mu_c / \alpha_1^2. \tag{39}$$

This recovers the scaling trends of previous predator-prey models. The flow is given by

$$|V''| = \gamma_L / \alpha_1. \tag{40}$$

Note that in this strongly frictional regime, the flow does not explicitly depend on frictional flow damping, which is the same as for previous results. In this regime, zonal flows are driven by the turbulence, and thus the flow curvature scales as $|V''| \sim \gamma_L$. The turbulence

energy here is controlled by both the linear drive and the flow damping. As a consequence, the near-marginal state can be achieved by decreasing the linear forcing of the turbulence. Therefore, zonal flow is weak, and thus the flow scale is large, in near-marginal (i.e., γ_L approaches zero) turbulence with strong frictional drag.

The new predator–prey model presented here does not depend sensitively on the specific turbulence type. For comparison with the results calculated from the zonal vorticity equation, we now use drift wave instability as an example. The coefficients are

$$\alpha_1 = \frac{k_y^2 \rho_s c_s}{L_n} \left(\tau_{ck} - \frac{1}{k_\parallel^2 D_\parallel} \frac{k_y^2 \rho_s^2 + L_m^{-2} \rho_s^2}{1 + k_y^2 \rho_s^2 + L_m^{-2} \rho_s^2} \right), \tag{41}$$

$$\alpha_2 = k_y^2 \rho_s^2 \tau_{ck}. \tag{42}$$

In the frictionless regime, the stationary zonal vorticity emerges as

$$|V''| = \frac{\alpha_1}{\alpha_2} = \frac{c_s}{\rho_s L_n} \left(1 - \frac{1}{\tau_{ck} k_\parallel^2 D_\parallel} \frac{k_y^2 \rho_s^2 + L_m^{-2} \rho_s^2}{1 + k_y^2 \rho_s^2 + L_m^{-2} \rho_s^2} \right), \tag{43}$$

which is consistent with Eq. (26). Vorticity gradient measures the jump across the flow shear field. Thus, the ZF profile can be deduced from the zonal vorticity by specifying boundary conditions. As shown by Fig. 4, for zonal flows, vorticity is equal to shear, which is of greater interest than the flow velocity.

In the strongly frictional regime, the zonal flow curvature is determined by $|V''| = \gamma_L / \alpha_1$. Next, we show that zonal flows are weak for drift wave turbulence. In the relevant limit of near-adiabatic electrons, i.e., $\tau_{ck} k_\parallel^2 D_\parallel \gg 1$, we obtain $\alpha_1 \cong \tau_{ck} k_y^2 \rho_s c_s / L_n$ to leading order. As a result, the zonal flow curvature is

$$|V''| \sim \frac{c_s}{\rho_s L_n} \frac{1}{\tau_{ck} k_\parallel^2 D_\parallel} \frac{k_y^2 \rho_s^2 + L_m^{-2} \rho_s^2}{(1 + k_y^2 \rho_s^2 + L_m^{-2} \rho_s^2)^3}. \tag{44}$$

Using the mixing length model, we determine the zonal flow scale in the strongly frictional regime, which is $L_{ZF} \sim (\tau_{ck} k_\parallel^2 D_\parallel K)^{2/3} f^{1/6} (1-f)^{1/6} \rho_s^{2/3} l_0^{1/3}$, where $K \equiv (1 + k_y^2 \rho_s^2 + L_m^{-2} \rho_s^2)^3 / (k_y^2 \rho_s^2 + L_m^{-2} \rho_s^2)$. The zonal flow shear is then $|\langle v_y \rangle'| \sim (\tau_{ck} k_\parallel^2 D_\parallel K)^{-1/3} f^{1/6} (1-f)^{1/6} \frac{c_s}{L_n} \left(\frac{l_0}{\rho_s} \right)^{1/3}$. Therefore, the zonal flow shear in the strongly frictional regime is weaker, and the scale is larger, than that in the frictionless regime, in the limit of near-adiabatic

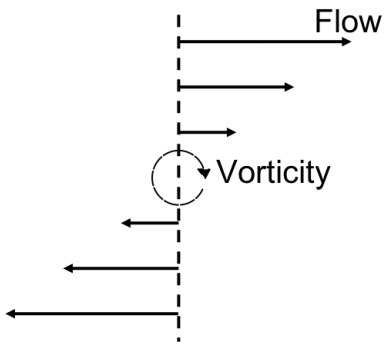

FIG. 4: For zonal flows, vorticity is equal to flow shear.

electrons, i.e., $\tau_{ck} k_\parallel^2 D_\parallel \gg 1$.

In the strongly frictional regime, the zonal flow scale is sensitive to wave-numbers, in both limits of $\tau_{ck} k_\parallel^2 D_\parallel \gg 1$ and $\tau_{ck} k_\parallel^2 D_\parallel \sim 1$. Again, the case of hydrodynamic limit requires further studies, which are beyond the scope of this paper. Note that collisional friction competes with drift wave frequency (which is roughly equal to decorrelation rate) in determining the plasma regimes, i.e., μ_c vs. $\omega_k \sim \omega_{*e} = k_y \rho_s c_s / L_n$. Therefore, shorter wavelength, and thus larger wave-number $k_y \rho_s$, favors the frictionless regime.

IV. DISCUSSION

In this paper, we study how wave–flow resonance affects the linear stability of drift wave turbulence, and how it regulates zonal flow saturation in the frictionless regime by resonant vorticity mixing. The main results of this paper are:

- Resonance stabilizes drift waves due to wave absorption. Counter-intuitively, flow shear can destabilize drift wave by weakening the resonance. This contradicts the conventional wisdom of shearing effects.

- Resonance opens a new channel of zonal flow saturation, absent frictional drag, through the irreversible turbulent mixing of vorticity. The scale of the stationary flow that forms is mesoscopic, but weighted somewhat more strongly toward microscale than macroscale. We show directly from analysis that the zonal flow scale is $L_{ZF} \sim f^{3/16}(1-f)^{1/8} \rho_s^{5/8} l_0^{3/8}$ in the relevant adiabatic regime (i.e., $\tau_{ck} k_\parallel^2 D_\parallel \gg 1$). The flow shear scales as $|\langle v_y \rangle'| \sim f^{3/16}(1-f)^{1/8} \frac{c_s}{L_n} \left(\frac{l_0}{\rho_s}\right)^{3/8}$.

- We calculate the degree of gyro-Bohm breaking and show that the resulting turbulent diffusivity is closer to the Bohm limit, i.e., $D \sim D_B \rho_*^{1/4} (l_0/L_n)^{3/4} \sim D_B \rho_*^{1/4}$. The base state mixing length, absent flow shear, is $l_0 \sim L_n$.

- We incorporate the saturation by mixing of vorticity into the predator–prey model. In contrast to previous results, the saturated flow is independent of the turbulence level, to leading order, in the frictionless regime. Thus, it can be significant for the relevant case of near-marginal turbulence. The turbulence energy is determined by the balance of linear drive and nonlinear dissipation without involving flow damping, and gives $E \sim \gamma_L^2/\varepsilon_c^2$.

In the presence of strong resonance, flow shear can linearly destabilize the drift wave turbulence, which is opposite to what the conventional shear suppression models predict. Resonance suppresses the instability as a result of wave absorption, and the flow shear can weaken the resonance. Therefore, wave-flow resonance is an important factor to be considered when studying the shear flow effect on stability, and on quasilinear fluxes that transport particle, vorticity, and momentum.

The Dimits up-shift regime spans low to zero collisionality and consists of weak turbulence near marginality. ZF saturation induced by resonant PV mixing is effective in both the frictionless regime and for near-marginal turbulence, and thus is compatible with the physics of the Dimits up-shift regime. Resonance regulates ZF saturation in the frictionless regime without the need to invoke tertiary instability. The saturated flow does *not* depend on the turbulence intensity. Hence, there can be significant zonal flows for near-marginal turbulence, absent frictional damping.

The stationary flow profile is determined by the balance between residual vorticity flux and the resonant diffusivity of vorticity. While ZF scale is often *assumed*, the new model discussed here *calculates* the saturated flow scale in the frictionless limit. In the limiting case with near-adiabatic electrons (i.e., $\tau_{ck} k_\parallel^2 D_\parallel \gg 1$), the ZF scale is mesoscopic, i.e., $L_{ZF} \sim f^{3/16}(1-f)^{1/8} \rho_s^{5/8} l_0^{3/8}$, in accordance with conventional assumptions. The mixing length regulated by the zonal flow shear is then $l_{mix} \sim \rho_s^{1/4} l_0^{3/4} \sim \rho_s^{1/4} L_n^{3/4}$. This implies a Bohm-like scaling of turbulent diffusivity, i.e. $D \sim D_B l_{mix}/L_n \sim D_B \rho_*^{1/4} (l_0/L_n)^{3/4} \sim D_B \rho_*^{1/4}$, where D_B is the Bohm diffusivity and $\rho_* \equiv \rho_s/L_n$. Note that absent zonal flow shear, the scaling is purely Bohm, i.e., $l_{mix} \sim l_0 \sim L_n$ and $D \sim D_B$. As a result of zonal flow shear,

the diffusivity scaling exhibits a gyro-Bohm correction, but weighted more toward Bohm. The scaling takes into account zonal flow shears that are self-consistently determined by shearing feedback on mixing length. Thus, externally driven flow shear may be needed to achieve scalings that are more gyro-Bohm. The flow shear driven by external power sources can reduce the mixing scale through shearing feedback. In addition, increasing the external power input can lead to the formation of transport barriers[15]. The transport barrier so formed could also reduce the mixing scale and thus could make the diffusivity weighted more toward gyro-Bohm.

We have derived an extended predator–prey model, incorporating the resonant PV mixing process. This new model is effective in the near-marginal turbulence. Thus, it can describe zonal flow saturation in the Dimits up-shift regime. In the frictionless regime, the resonant diffusion of vorticity leads to nonlinear saturation of zonal flow. The turbulence energy is saturated by nonlinear enstrophy dissipation tied to forward cascade of potential enstrophy. As a result, the turbulence energy scales with the linear forcing rate as $E \sim \gamma_L^2$. The saturated flow does *not* depend on the turbulence intensity. Hence, there can be significant flows in near-marginal turbulence. Therefore, frictionless ZF saturation by resonant PV mixing is expected to be effective in weak turbulence regimes. In the frictional regime with significant frictional flow damping, the dependence of turbulence energy level on flow damping is recovered. The flow is driven by turbulence, while saturated by collisions. Hence, in this limit, the flow is very weak in near-marginal turbulence. Note that in the frictionless regime, the zonal flow structure does not depend on turbulence properties, such as wave-numbers, in the relevant near-adiabatic limit. In the strongly frictional regime, the zonal flow scale is sensitive to wave-numbers. Shorter wavelength, and thus larger wave-number $k_y\rho_s$, favors the frictionless regime.

The model discussed here addresses the long-standing question of "how close is 'close'" in near-marginal systems. It is effective in both near-marginal turbulence and in the frictionless regime. Thus, when expanded to *1D*, it can be used to study avalanches and staircase formation[19, 20]. In 1D, avalanching induces variability of profiles, and thus of local growth rates. The scaling $E \sim \gamma_L^2$ suggests a variability-dominated state can result when $\gamma_L \to 0$. This follows because γ_L has an exponent > 1, which holds true as long as the self-saturation of fluctuation PE exhibits the dependence $\varepsilon_c\Omega^{1+p}$, where $0 < p < 1$. Thus, the scaling of E with γ_L is stronger than the conventional weak turbulence result. The local linear growth

rate is then set by both equilibrium (mean) and variable (i.e., avalanche-induced) profile gradients, i.e., $\gamma_L = \overline{\gamma}_L + \tilde{\gamma}_L$. As a result of resonant PV mixing in the frictionless regime, the turbulence state is determined by $E \sim \gamma_L^2 \sim \overline{\gamma}_L^2 + \tilde{\gamma}_L^2$. $\overline{\gamma}_L$ is determined by the difference between mean profile gradient and critical gradient. In near-marginal turbulence, the mean gradient approaches the critical gradient, so $\overline{\gamma}_L \to 0$. Thus, there the turbulence state is primarily controlled by noise from avalanche variability, i.e., $E \sim \tilde{\gamma}_L^2 \gg \overline{\gamma}_L^2$. Such noise is produced by avalanching, which stochastically modulates the driving gradient. In this case, the predator–prey model must be treated as a set of coupled stochastic differential equations. In 1D, the relevant system is a nonlinear reaction–diffusion model like that of Eq. (22) and (23), including multiplicative noise. The results in this work thus define the boundary for "marginality". The turbulence energy scales with the dimensionless ratio $(\gamma_L/\varepsilon_c)^2$, where ε_c is the dissipation rate of PE. Therefore, the turbulence can be "marginal" when the equilibrium growth rate $\overline{\gamma}_L < \varepsilon_c$. This gives a basis upon which to define the extent of the "near-marginal regime".

Acknowledgments

The authors are grateful to Z. B. Guo, A. Ashourvan, H. Che, R. Z. Sagdeev, X. Q. Xu, G. R. Tynan for insightful discussions. We also acknowledge the useful and interesting discussions at the Festival de Théorie. This work was supported by the U.S. Department of Energy, Office of Science, OFES, under Award Number DE-FG02-04ER54738.

---

[1] P. H. Diamond, S. I. Itoh, K. Itoh, and T. S. Hahm, Plasma Physics and Controlled Fusion **47**, R35 (2005).

[2] Ö. D. Gürcan and P. H. Diamond, Journal of Physics A: Mathematical and Theoretical **48**, 293001 (2015).

[3] P. H. Diamond, Y.-M. Liang, B. A. Carreras, and P. W. Terry, Phys. Rev. Lett. **72**, 2565 (1994).

[4] S. Kobayashi, Ö. D. Gürcan, and P. H. Diamond, Physics of Plasmas **22**, 090702 (2015).

[5] G. McKee, C. Petty, R. Waltz, C. Fenzi, R. Fonck, J. Kinsey, T. Luce, K. Burrell, D. Baker, E. Doyle, et al., Nuclear Fusion **41**, 1235 (2001).

[6] M. Xu, G. R. Tynan, P. H. Diamond, C. Holland, J. H. Yu, and Z. Yan, Phys. Rev. Lett. **107**, 055003 (2011).

[7] L. Cui, A. Ashourvan, S. C. Thakur, R. Hong, P. H. Diamond, and G. R. Tynan, Physics of Plasmas **23**, 055704 (2016).

[8] X. Wang, P. H. Diamond, and M. N. Rosenbluth, Physics of Fluids B: Plasma Physics **4**, 2402 (1992).

[9] F. L. Waelbroeck, T. M. A. Jr., P. N. Guzdar, and A. B. Hassam, Physics of Fluids B: Plasma Physics **4**, 2441 (1992).

[10] B. A. Carreras, K. Sidikman, P. H. Diamond, P. W. Terry, and L. Garcia, Physics of Fluids B: Plasma Physics **4**, 3115 (1992).

[11] Z. B. Guo, T. S. Hahm, and P. H. Diamond, Physics of Plasmas **22**, 122304 (2015).

[12] Z. B. Guo and P. H. Diamond, Phys. Rev. Lett. **117**, 125002 (2016).

[13] B. N. Rogers, W. Dorland, and M. Kotschenreuther, Phys. Rev. Lett. **85**, 5336 (2000).

[14] E.-J. Kim and P. H. Diamond, Physics of Plasmas **9**, 4530 (2002).

[15] P. Mantica, C. Angioni, C. Challis, G. Colyer, L. Frassinetti, N. Hawkes, T. Johnson, M. Tsalas, P. C. deVries, J. Weiland, et al., Phys. Rev. Lett. **107**, 135004 (2011).

[16] A. M. Dimits, T. J. Williams, J. A. Byers, and B. I. Cohen, Phys. Rev. Lett. **77**, 71 (1996).

[17] A. Galeev, R. Sagdeev, V. Shapiro, and V. Shevchenko, Zhurnal Eksperimental'noi i Teoreticheskoi Fiziki **73**, 1352 (1977).

[18] H. Che, M. L. Goldstein, P. H. Diamond, and R. Z. Sagdeev, Proceedings of the National Academy of Sciences **114**, 1502 (2017).

[19] G. Dif-Pradalier, P. H. Diamond, V. Grandgirard, Y. Sarazin, J. Abiteboul, X. Garbet, P. Ghendrih, A. Strugarek, S. Ku, and C. S. Chang, Phys. Rev. E **82**, 025401 (2010).

[20] D. E. Newman, B. A. Carreras, P. H. Diamond, and T. S. Hahm, Physics of Plasmas **3**, 1858 (1996).

[21] A. Ashourvan and P. H. Diamond, Phys. Rev. E **94**, 051202 (2016).

[22] A. Ashourvan and P. H. Diamond, Physics of Plasmas **24**, 012305 (2017).

[23] W. M. Manheimer and T. H. Dupree, The Physics of Fluids **11**, 2709 (1968).

[24] G. I. Taylor, Philosophical Transactions of the Royal Society of London. Series A, Containing Papers of a Mathematical or Physical Character **215**, 1 (1915).

[25] P. H. Diamond and Y. Kim, Physics of Fluids B: Plasma Physics **3**, 1626 (1991).

[26] H. Biglari, P. H. Diamond, and P. W. Terry, Physics of Fluids B: Plasma Physics **2**, 1 (1990).

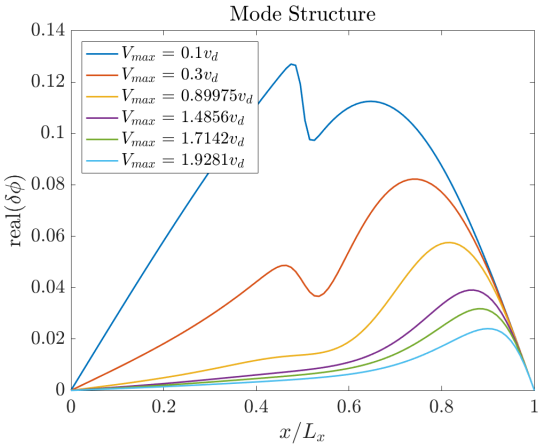

FIG. 5: Mode structure for various flow magnitudes, with fixed flow shear. The flow is given by function $V_y = V_{max} \tanh\left[(x - 0.5L_x)/L_V\right]$.

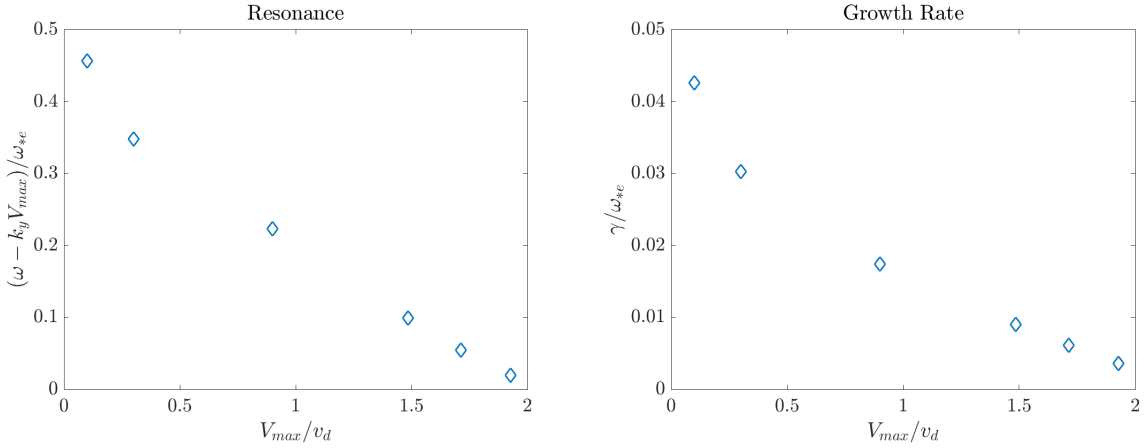

FIG. 6: Resonance (left) and growth rate (right) vs. flow magnitude, with fixed shear. The flow is given by function $V_y = V_{max} \tanh\left[(x - 0.5L_x)/L_V\right]$.

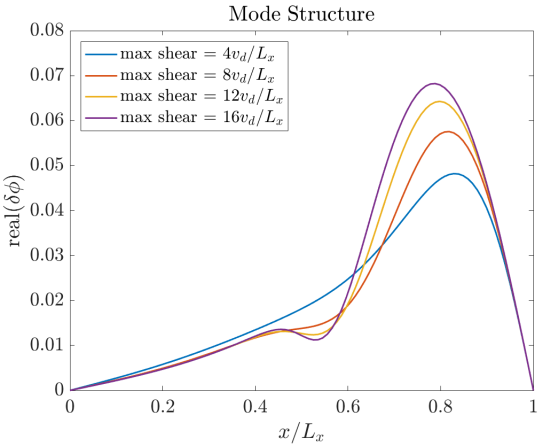

FIG. 7: Mode structure for various flow shears, with fixed flow amplitude. The flow is given by function $V_y = V_{max} \tanh\left[(x - 0.5L_x)/L_V\right]$.

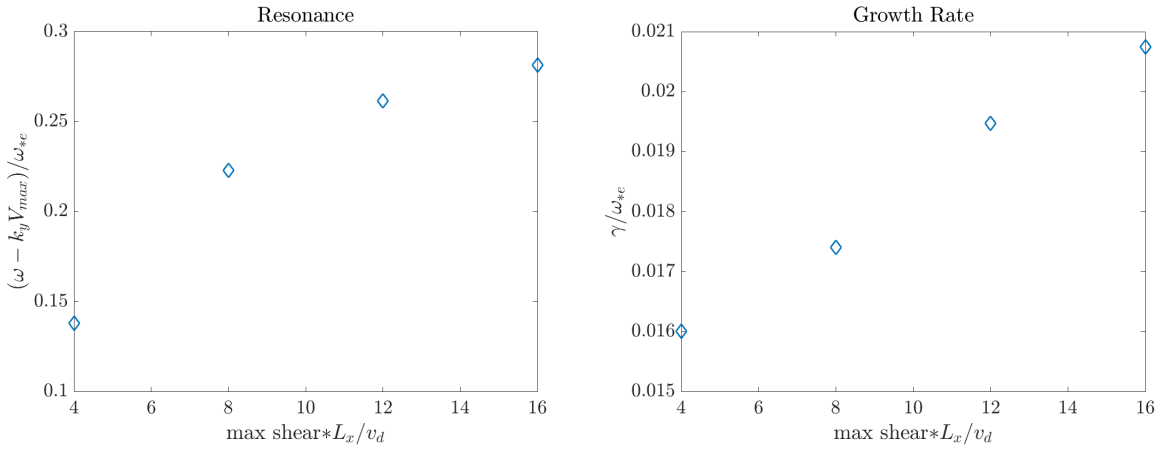

FIG. 8: Resonance (left) and growth rate (right) vs. flow shear, with fixed magnitude. The flow is given by function $V_y = V_{max} \tanh\left[(x - 0.5L_x)/L_V\right]$.